Turkish Journal of Chemistry
http://journals.tubitak.gov.tr/chem/
Research Article

Turk J Chem
(2014) 38: 568 – 580

doi:10.3906/kim-1308-35

Selective CO methanation over CeO_2–ZrO_2-composed NiO and Co_3O_4 catalysts

Filiz BALIKÇI DEREKAYA*, Derya MERCAN ERMERGEN
Advanced Technologies Department, Institute of Science, Gazi University, Ankara, Turkey

Received: 14.08.2013 • **Accepted:** 22.12.2013 • **Published Online:** 11.06.2014 • **Printed:** 10.07.2014

Abstract: CeO_2–ZrO_2-composed NiO and Co_3O_4 catalysts were prepared by 3 different methods. Both CO methanation and selective CO methanation were carried out. All catalysts were prepared by (1) co-precipitation, (2) surfactant-assisted co-precipitation, and (3) surfactant-assisted co-precipitation with ultrasound mixing methods. Catalysts were characterized by using N_2 physisorption, XRD, SEM, TEM, and TPR-H_2 techniques. The highest surface area value, uniform pore size distribution, and pores having small diameters were observed for the catalysts prepared by using the surfactant and ultrasound. The $NiO/CeO_2/ZrO_2$ prepared by the surfactant-assisted co-precipitation was the most active catalyst for CO methanation. It gave 50% CO conversion to CH_4 at 150 °C and all CO was converted to CH_4 after T > 225 °C. Moreover, 22.3% CH_4 was formed and the CO level decreased below 100 ppm at 200 °C during the selective CO methanation activity test over this catalyst.

Key words: Surfactant, ultrasound, CeO_2–ZrO_2, methanation

1. Introduction

The H_2–CO–CO_2 gas mixture has been used in the synthesis of different chemicals and also as an air gas. The gasification of coal gives a similar gas mixture. Since steam reforming gas has low energy per volume and contains poisonous CO gas, this H_2–CO–CO_2 gas mixture should be converted to methane, which has higher energy density, in order to be used as a fuel. Since the main components are hydrogen, carbon monoxide, and carbon dioxide, the methane can be formed by the methanation of carbon monoxide and carbon dioxide.[1]

$$CO + 3H_2 \rightarrow CH_4 + H_2O$$
$$CO_2 + 4H_2 \rightarrow CH_4 + 2H_2O$$

There is a need for a catalyst that has high activity and resistance in order to convert carbon monoxide selectively to methane. The studies in the literature showed that mostly Ni/Al_2O_3, Ni/SiO_2, Ru/SiO_2, Co/γ-Al_2O_3, Ni/ZrO_2, Ru/TiO_2, Ru/Al_2O_3, and Ru/ZrO_2 catalysts were used for methanation.[2–5] CeO_2 and ZrO_2 are used as catalyst components in order to improve properties of catalysts. CeO_2 provides oxygen to the catalyst's surface, which makes metal dispersion more stable. Addition of ZrO_2 to CeO_2 improves CeO_2's redox properties, oxygen-storage capacity, and thermal resistance.[6] Nickel and cobalt oxide are used as active materials in the catalyst in this study. Cobalt is a cheaper catalytic active material than Ru and Rh.[7] The interaction between cobalt and ceria affects the morphological and redox properties of the composite oxides.[8]

The catalyst preparation method has important effects on the final catalyst properties, such as surface area, pore diameter, pore volume, and activity. Sol-gel, co-precipitation, and impregnation are the most

*Correspondence: filizb@gazi.edu.tr

common techniques to prepare catalysts.[2,3,9–11] In recent studies, materials called surfactants were used in the preparation techniques mentioned above to obtain catalysts with better properties. These surfactants lead to many improvements in nanosized catalysts. These catalysts have uniform pore diameters and therefore high activities for the desired reactions.[12–17] The parameters used in the preparation stages are as important as the materials used in the catalyst preparation. In general, mechanical mixing is used at the aging stage. In some studies, ultrasound was used to mix the precursor solutions that were used during the catalyst preparation. Finally, the best results were obtained from catalysts prepared by ultrasound mixing.[18–20]

The aim of this study was to develop 2 different catalysts that show high activity both in the CO methanation and selective CO methanation reactions. The first catalyst was a mixture of NiO, CeO_2, and ZrO_2. The second catalyst was a mixture of Co_3O_4, CeO_2, and ZrO_2. Hence 2 different catalysts were prepared as follows: 50/25/25 (mol %) $NiO/CeO_2/ZrO_2$ and 50/25/25 (mol %) $Co_3O_4/CeO_2/ZrO_2$. Catalysts were prepared by using 3 different preparation methods. All 3 methods are based on precipitation but the procedures are different. The methods were called (1) co-precipitation (C), (2) surfactant-assisted co-precipitation (S), and (3) surfactant-assisted co-precipitation with ultrasound mixing (U). The resultant effects of the surfactant and ultrasound were determined.

2. Results and discussion

2.1. Catalyst characterization results

2.1.1. X-ray diffraction (XRD)

Figure 1 shows the XRD spectra collected from all catalysts after calcination. The characteristic peaks of CeO_2, ZrO_2, and CeZroxide are evident in all $NiO/CeO_2/ZrO_2$ and $Co_3O_4/CeO_2/ZrO_2$ samples. The CeO_2 peaks were observed at $2\theta = 29.4^\circ$, 33.5°, 47.4°, 56.8°, 48.1°, 48.8°, and 56.8°. The ZrO_2 peaks were observed at $2\theta = 31.7^\circ$, 36.6°, 38.3°, 50.7°, 60°, 74.3°, and 88.6°. The peaks corresponding to the CeZroxide phase were observed at $2\theta = 28.5^\circ$, 33°, 48°, 56.6°, 69°, 71°, 77.3°, 78.5°, and 88.3°. The Co_3O_4 crystal phase was obtained in addition to the CeO_2, ZrO_2, and CeZroxide phases on the CoCeZr catalysts. The Co_3O_4 peaks were observed at $2\theta = 31.4^\circ$, 36.9°, 44.9°, 59.2°, and 65.4°. The NiO peaks were observed at $2\theta = 37.2^\circ$, 43.4°, and 63.1° on the NiCeZr catalysts in addition to the CeO_2, ZrO_2, and CeZroxide phases. The position of the peaks obtained can be supported by the data in the literature. Lin et al. indicated that the peaks at $2\theta = 28.64^\circ$ and 28.88° were the formation of CeO_2–ZrO_2 mixed oxide.[21] Khaodee et al. and Fischer et al. indicated that the peaks at $2\theta = 28.2^\circ$ and 31.5° were assigned to the monoclinic phase in ZrO_2 and the peak at $2\theta = 30.2^\circ$ was the characteristic peak of the tetragonal phase in ZrO_2.[22,23] They also indicated that the cubic fluorite phase in CeO_2 gave diffraction peaks at $2\theta = 28.6^\circ$ and 33.1°. Takeguchi et al. reported that the peaks at 37° and 43° are responsible for the NiO phase.[24] Asencios et al. also confirmed the Bragg angle of NiO phase observed in this study.[25]

Table 1. Textural and structural properties of the catalysts.

Catalysts	Surface area m^2/g			$V_{micro+meso}$ pore volume (liquid N_2 cc/g)			V_{total} pore volume (liquid N_2 cc/g)			Average pore diameter (nm)		
	Preparation methods											
	C[3]	**S**[4]	**U**[5]	**C**	**S**	**U**	**C**	**S**	**U**	**C**	**S**	**U**
CoCeZr[1]	65	27	102	0.347	0.084	0.216	0.415	0.101	0.236	17.5	4.2, 12.2	3.3, 9.3
NiCeZr[2]	66	107	105	0.427	0.204	0.233	0.483	0.211	0.236	31.3	3.4, 16.8	4.9, 16.8

[1] $Co_3O_4/CeO_2/ZrO_2$, [2] $NiO/CeO_2/ZrO_2$, [3] Co-precipitation, [4] Surfactant-assisted co-precipitation, [5] Surfactant-assisted co-precipitation with ultrasound mixing.

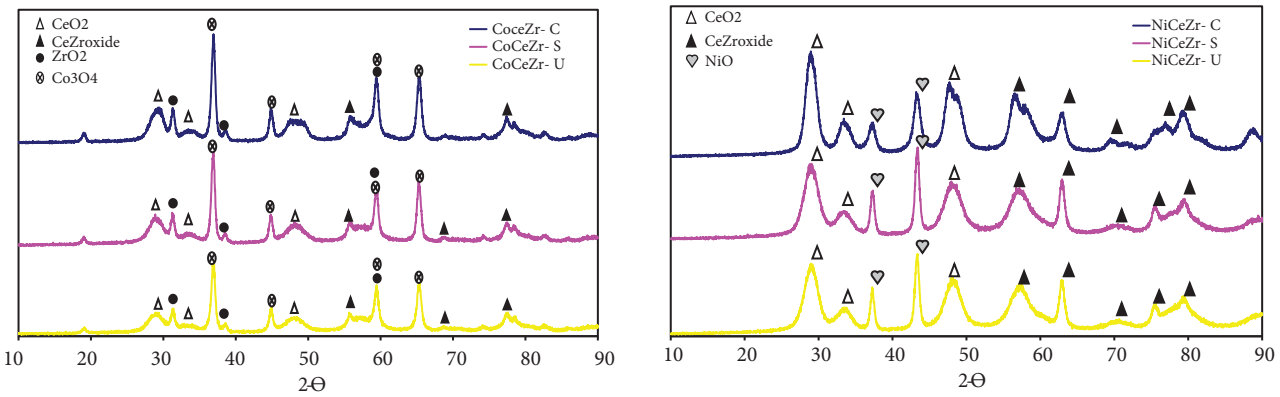

Figure 1. XRD diagrams of the catalysts.

2.1.2. Nitrogen physisorption measurements

Nitrogen adsorption desorption isotherms of the catalysts were obtained from the N_2 physisorption analysis. Catalysts showed different hysteresis behaviors. According to the IUPAC classification, Type IV and Type V adsorption isotherms were obtained. The CoCeZr–C and NiCeZr–C, which were prepared by the 3 methods, showed a Type V adsorption desorption isotherm. A Type V isotherm is obtained from porous adsorbents. The CoCeZr and NiCeZr catalysts, which were prepared by the S and U methods, showed a Type IV adsorption desorption isotherm. This type of isotherm is obtained from mesoporous adsorbents.[26] According to the shape of the hysteresis, the shape of the structure can be estimated. Catalysts prepared by the co-precipitation method showed Type H3 hysteresis, which is observed with aggregates at plate-like particles, giving rise to slit-shaped pores.[27–29]

Multipoint BET surface areas of the catalysts are shown in Table 1. The best surface area values were obtained from the catalysts prepared by the U method. In comparison with the C method, results showed that the surfactant has great effect on the surface area. CTAB played an important role in controlling the phase structure and morphology of the product.[30,31] In addition, Hernandez et al. explained that surfactant-assisted synthesis leads to the formation of solids with narrow and monomodal pore size distributions.[32] By combination of surfactant CTAB with ultrasound mixing, the surface area values of the catalysts further increased. Boffito et al. reported that increases in acidity and surface area were observed by using ultrasound.[33] They indicated that the improvement in the properties of the catalysts is probably due to the effects generated by acoustic caviation. The average pore sizes of the catalysts are listed in Table 1. All catalysts had mesopores (2 nm $<$ d $<$ 50 nm). Pore sizes of the catalysts varied with the preparation method type. The surfactant and ultrasound have significant effects on the pore sizes of the catalysts. Smaller pore sizes and more uniform pore size distribution were obtained with the S and U methods. Ultrasound promotes nucleation of crystals, and accelerates and depresses agglomeration. Hence materials that have narrow pore size distribution can be produced.[34–36]

2.1.3. Temperature programmed reduction (TPR-H_2)

Temperature programmed reduction studies were carried out in order to determine the reduction temperatures of the catalysts and reducible species in the catalysts and also in order to determine the thermal treatment temperature used to activate catalysts. Since hydrogen existed in the reaction gas mixture, the behavior of the catalyst against the hydrogen was determined. TPR measurements were carried out over the CoCeZr and NiCeZr catalysts and are shown in Figure 2. The area under the TPR profile of the NiCeZr–C catalyst is the

highest one (Figure 2). The TPR profiles of the catalysts prepared by the S and U methods were very similar. Catalyst prepared by the C method gave 1 broadening reduction peak that had 2 maxima at 397 °C and 450 °C and gave a narrow size reduction peak at 522 °C. Catalysts prepared by the S and U methods gave a narrow size reduction peak at 350 °C. The reduction peak at the temperature interval between 397 °C and 550 °C is due to the reduction of NiO, which is strongly interacting with CeO_2–ZrO_2.[37–39] The reduction peak obtained at 522 °C is due to the reduction of the NiO phase also.[38,40,41] Depending on the strength of the interaction between the CeO_2 and ZrO_2, the shape and the position of the TPR profiles varies.[40] Figure 2 shows the TPR-H_2 results of the CoCeZr catalysts. CoCeZr–C catalyst gave 2 reduction peaks at 301 °C and 573 °C. CoCeZr–S catalyst gave a more broadening reduction peak at 650 °C with a corner. CoCeZr–U catalyst gave 3 reduction peaks at 350 °C, 488 °C, and 619 °C. The reduction of Co_3O_4 took place in 3 steps. Firstly Co_3O_4 was reduced to CoO (100 °C–350 °C) and then CoO was reduced to Co (T > 350 °C).[37,42] According to the literature, the reduction peaks obtained at low temperature can be attributed to the reduction of Co_3O_4 to CoO and the reduction peak at high temperature can be attributed to the reduction of the CoO phase to Co. The reduction peak at high temperature may also be due to the reduction of the CeZroxide phase.[42]

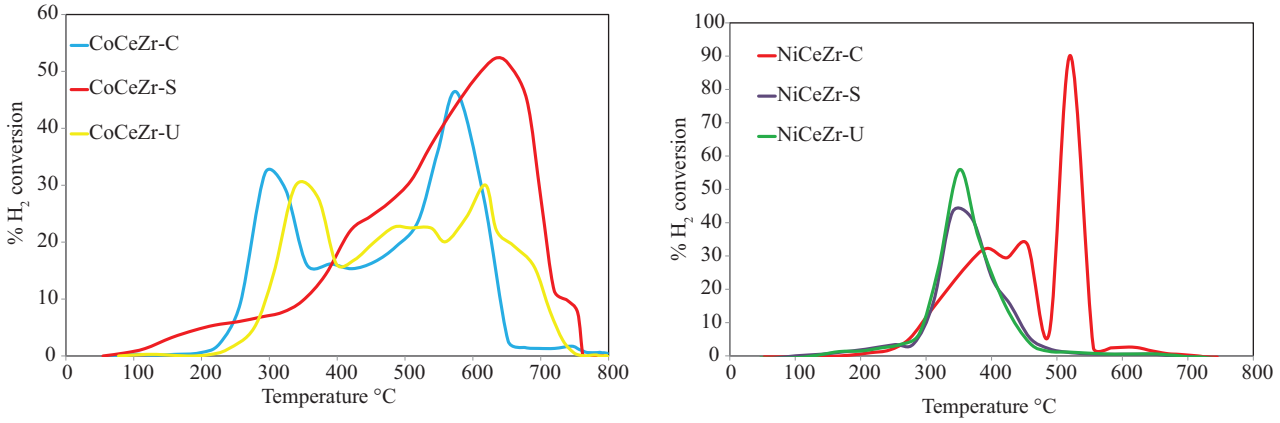

Figure 2. TPR-H_2 profiles of the CoCeZr and NiCeZr catalysts.

2.1.4. Scanning electron microscopy (SEM)

SEM micrographs were obtained over the CoCeZr and NiCeZr catalysts (Figure 3). The catalysts gave spherical particles. It was observed that particle sizes were almost the same. In comparison with the CoCeZr catalysts, the gaps between the particles were small and the average particle size was small on the NiCeZr catalysts. The SEM images show that the catalysts' preparation method did not significantly affect the shape or size of the particles. The weight percentages of components obtained from the EDX analysis are given in Table 2. EDX analysis showed the cobalt, nickel, and cerium weight percentages are greater than the desired ones and the zirconia weight percentage is smaller than the desired one.

2.1.5. Transmission electron microscopy (TEM)

The morphology of the NiCeZr and CoCeZr catalysts, which were prepared by the surfactant-assisted co-precipitation method, is shown in Figures 4a and 4b. From the TEM image of the CoCeZr catalyst, large particles are observed (Figure 4a). The catalyst displays some surface agglomeration of Co_3O_4 nanoparticles with a uniform particle size distribution. The particle size of Co_3O_4 was between 12.5 and 24 nm tested by

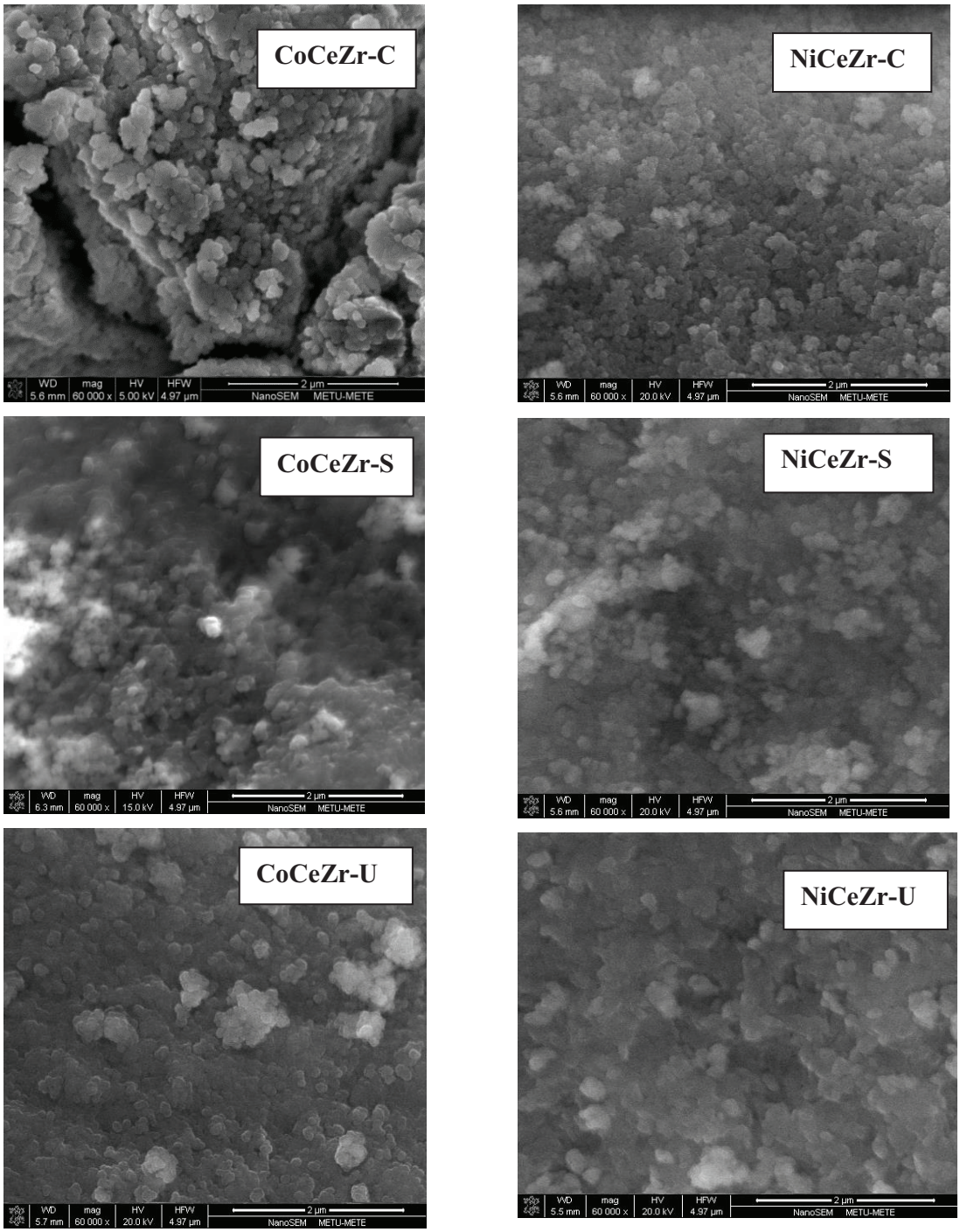

Figure 3. SEM images of the catalysts.

the TEM. It is obvious that the TEM image of the NiCeZr catalyst in Figure 4b shows that NiO crystallites are not well distributed and aggregation is observed alongside different particle shapes (rod, polyhedron, cube). The crystallite sizes of NiO species in the $NiO/CeO_2/ZrO_2$ catalyst were estimated from the TEM image to be between 11.6 and 24 nm. Yongzhao et al. pointed out the NiO agglomeration in the $NiO–SiO_2$ catalyst and they observed the NiO particle size to be 15–20 nm, which is very close to our results.[43]

Table 2. SEM-EDX analysis of the catalysts.

Catalyst	Preparation method	Ni	CoK	CeL	ZrL
NiCeZr	C	36.99	-	45.59	17.42
	S	39.45	-	45.53	15.02
	U	34.91	-	47.57	17.52
CoCeZr	C	-	65.72	25.21	9.08
	S	-	67.08	26.40	6.52
	U	-	62.24	27.94	9.83

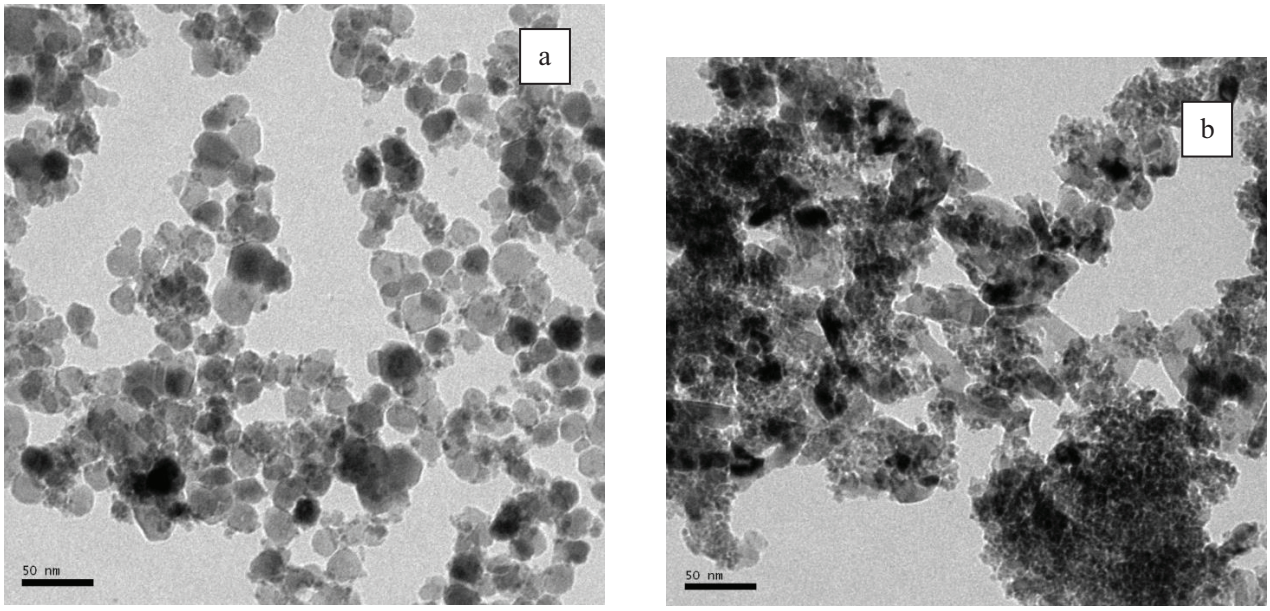

Figure 4. TEM images of the catalysts prepared by the surfactant-assisted co-precipitation method: (a) CoCeZr and (b): NiCeZr.

2.2. Catalytic activity results

Since the aim of the catalyst was to eliminate the CO in the reformer gas, which was a hydrogen-rich gas, catalytic activity studies for the CO methanation and selective CO methanation reactions were carried out. CO methanation reactions were performed between 125 °C and 375 °C. All catalysts were in-situ reduced before the CO methanation reaction by using pure H_2 at 500 °C for 1 h. The main active phases were changed after reduction. The nickel oxide reduced to Ni in the NiCeZr catalysts and cobalt oxide reduced to CoO and metallic Co in the CoCeZr catalysts. Catalytic activities of the catalysts as a function of the reaction temperature for the CO methanation reaction are shown in Figures 5 and 6. Among the CoCeZr catalysts, the best activity was obtained from the CoCeZr–S catalyst (Figure 5). It gave 50% conversion below 125 °C and all CO was converted above 175 °C. In addition, the methane formation behavior of the CoCeZr–S is not similar to the CO conversion behavior. This catalyst gave 100% CH_4 formation at 275 °C, but methane formation decreased with temperature after 275 °C. According to the TPR-H_2 results, the main active phase in CoCeZr catalysts is CoO. The oxide cobalt structure may lead to CO_2 formation because of the reaction between surface oxygen and gas phase CO. The tracer amount of CO_2 formation, detected in the experiments, depressed CH_4 formation, but an increase in temperature may accelerate CH_4 formation. Hence 100% CH_4 formation was obtained at

275 °C over the CoCeZr–S. The 50% conversion temperatures of the CoCeZr–C and CoCeZr–U catalysts were 201 °C and 175 °C, respectively. Both CoCeZr–U and CoCeZr–C gave 100% conversion above 225 °C. Over the CoCeZr–C and CoCeZr–U catalysts, methane formation increased with increasing reaction temperature. Between the CoCeZr–C and CoCeZr–U catalysts, methane formation started at a lower temperature over the latter. The methane formation values indicated that all CO converted to methane over the CoCeZr-C and CoCeZr-U catalysts. If the characterization results are combined with the activity results, it can be seen that while the highest activity was obtained over the CoCeZr–S the highest CH_4 formation was obtained over the CoCeZr–U, which had the highest surface area. Activity of the CoCeZr–U catalysts can be compared with the results obtained by Takenaka et al.[9] They studied CO methanation over $CoZrO_2$ catalyst. They observed only 48.2% CO conversion at 523 K, which is lower than that found in our study. The difference might be due to the cerium oxide. The combination effect between the CeO_2 and ZrO_2 might lead to an increase in activity.

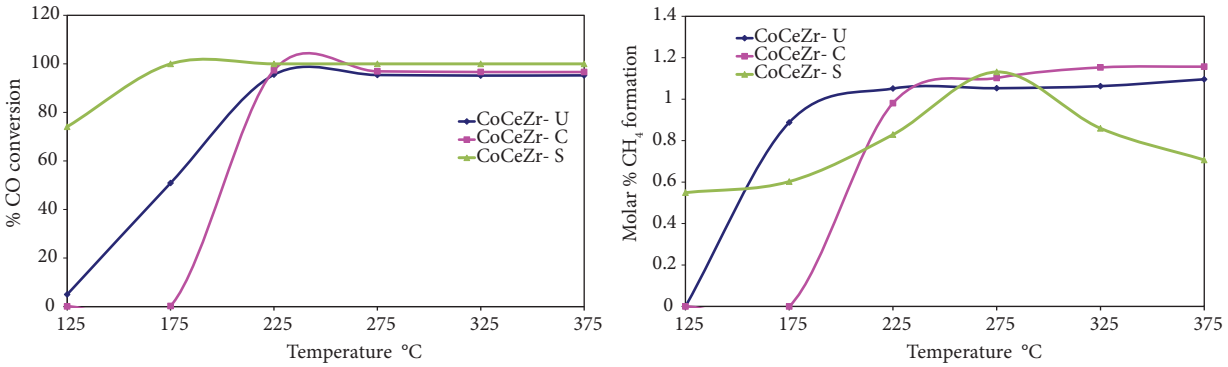

Figure 5. Activity results as a function of the temperature for the CO methanation over the CoCeZr catalysts (1% CO, 50% H_2, and rest He; S.V.: 45,000 h^{-1}; 25 mg of catalysts).

The CO methanation catalytic activity results of the NiCeZr catalysts are shown in Figure 6. The 50% CO conversion temperatures of NiCeZr–C, NiCeZr–S, and NiCeZr–U catalysts are 250 °C, 198 °C, and 193 °C, respectively. While all CO converted above the 225 °C over the NiCeZr–C and NiCeZr–S catalysts, 100% CO conversion was observed above 275 °C over the NiCeZr–U catalyst. Based on the activity results over NiCeZr catalysts, NiCeZr–S and NiCeZr–U were more active than NiCeZr-C. In addition, catalytic activities of the NiCeZr–U and NiCeZr–S catalysts were very close to each other.

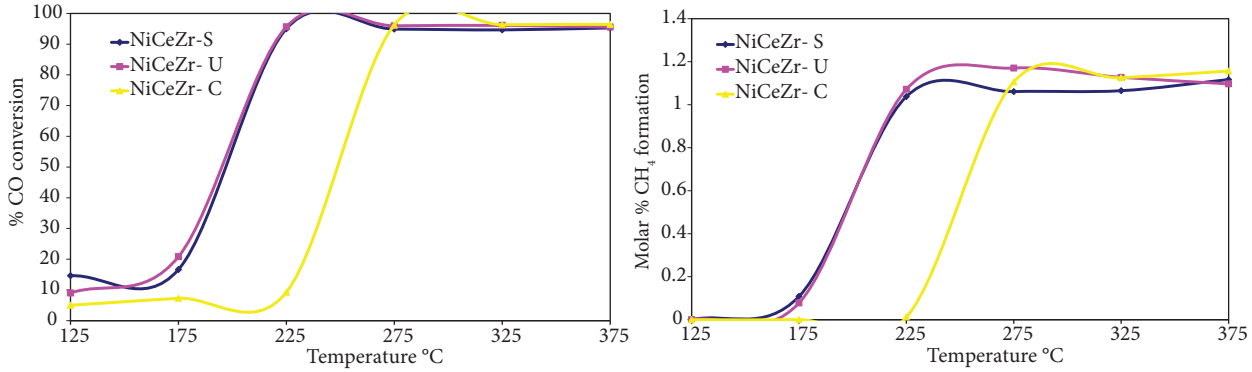

Figure 6. Activity results as a function of the temperature for the CO methanation over the NiCeZr catalysts (1% CO, 50% H_2, and rest He; S.V.: 45,000 h^{-1}; 25 mg of catalysts).

The carbon monoxide conversion curves and methane formation curves were very similar. This may have been due to the active phase structure. According to the TPR-H_2 results, nickel oxide converted to metallic Ni after 500 °C. Since the active phase structure was the same in all NiCeZr catalysts, similar results were obtained. According to the activity results, CTAB had a great effect on both characterization properties and hence activity properties of the NiCeZr catalysts. During the CO methanation catalytic activity tests of the NiCeZr catalysts, CO_2 was not observed in the effluent gas stream. This indicated that CO only converted to methane during the reaction. This result may have been due to the reduction of NiO to metallic Ni in all NiCeZr samples.

The component combined with cobalt oxide or nickel oxide has important effects on CO methanation activity. The interactions between the components affect the active phase distribution and thermal stability. Batista et al. studied CO methanation with Co/γ–Al_2O_3 catalyst.[44] Although they observed 90% CH_4 formation at 400 °C over Co/γ–Al_2O_3, at this temperature $Co_3O_4/ZrO_2/Al_2O_3$ catalysts gave 100% CO conversion to CH_4. This result shows the difference between the CeO_2-ZrO_2 and Al_2O_3 in CO methanation activity. The effects of ZrO_2 on CO methanation activity can be supported by several studies. Wu et al. studied the effect of the ZrO_2 promoter on the CO methanation activity of the Ni/SiO_2 catalysts.[45] They observed that the addition of ZrO_2 promoter enhanced the CO adsorption capacity, and in the presence of H_2 more bridged carbonyl hydrides were formed. The effect of ZrO_2 is also supported by Liu et al.[46] On the other hand, Wang et al. connected the high CO methanation activity of Ni/ZrO_2–SiO_2 catalyst to the high Ni dispersion.[47] They suggested that formation of a Si–O–Zr bond enhances the reduction degree of NiO species. Zhang et al. also indicated that the addition of ZrO_2 to Ni/Al_2O_3 catalysts led to an increase in CO methanation activity.[48] The preparation method, catalyst composition, and preparation parameters (i.e. pH, aging time, temperature, metal salt concentration, calcination temperature, type of surfactant) affect the catalytic activity and characterization results. If we compare the NiCeZr catalytic activity results with the 10 wt.% Ni/CeO_2 studied by Zyryanova et al. to see the effect of ZrO_2, we can see the enhancing effect of ZrO_2.[49] They observed that CO concentration in the effluent gas stream was below 10 ppm after the reaction between 250 and 300 °C over 10 wt.% Ni/CeO_2. At this temperature interval, we observed 100% CO conversion to methane over NiCeZr catalysts. This result also shows the effect of ZrO_2. According to Jiang et al., besides the ZrO_2, CeO_2 on the catalyst surface improves the interaction between active phase and support and dispersion of the active phase across the catalyst surface.[50] Habazaki et al. indicated that tetragonal ZrO_2 was responsible for the high activity to CO methanation, which was transformed to monoclinic ZrO_2 during the reaction and all CO converted to methane above 523 K.[1]

Selective methanation was carried out over the NiCeZr–S catalyst (Figure 7). The aim of our study was to reduce the CO in the reformer gas in order produce H_2-rich fuel for the PEMFC by selective methanation. Therefore, a selective methanation activity test was carried out. The feed was composed of 1% CO, 25% CO_2, 50% H_2, and the rest He, and the reaction temperature was increased from 100 to 600 °C. At 300 °C, ≈22.3% CH_4 formation was observed. The CH_4 formation decreased after 300 °C because of the reverse water gas shift reaction. CO_2 conversion started after 400 °C. CO was converted via selective CO methanation until 200 °C, at which CO composition was below 1%. According to the selective CO methanation catalytic activity result, NiCeZr–S gave low activity because of the reverse water gas shift reaction. The selective CO methanation reaction temperature was suggested to be in the range of 100–200 °C in order to convert CO to CH_4. CO concentration was reduced below 100 ppm at 200 °C. Similar results were given in the literature. Liu et al.

observed that CO concentration decreased under 20 ppm between 260 and 280 °C during the selective CO methanation reaction over the Ni/ZrO_2 catalyst.[51]

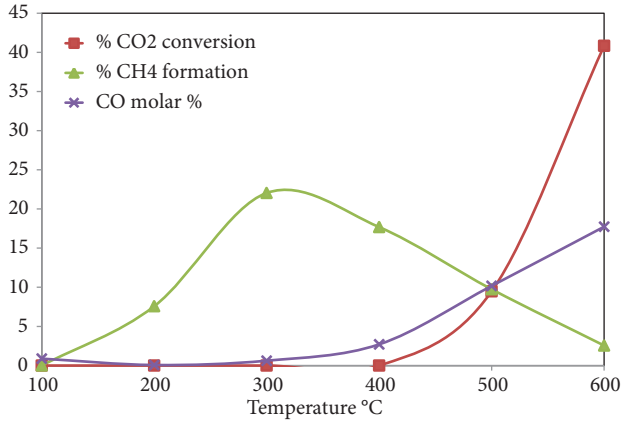

Figure 7. Activity results as a function of the temperature for the selective CO methanation over the NiCeZr-S (1% CO, 25% CO_2, 50% H_2, and rest He; S.V.: 45,000 h^{-1}; 25 mg of catalysts).

Deactivation studies were done over the NiCeZr–S catalyst. Activity of the catalyst was investigated at 300 °C for 300 min by using 1% CO, 25% CO_2, 50% H_2, and the rest He feed composition. During the deactivation test, catalytic activity of the catalyst did not change (Figure 8). The CO molar percentage, CO_2 molar percentage, methane formation, and H_2 conversion stayed stable during the experiment.

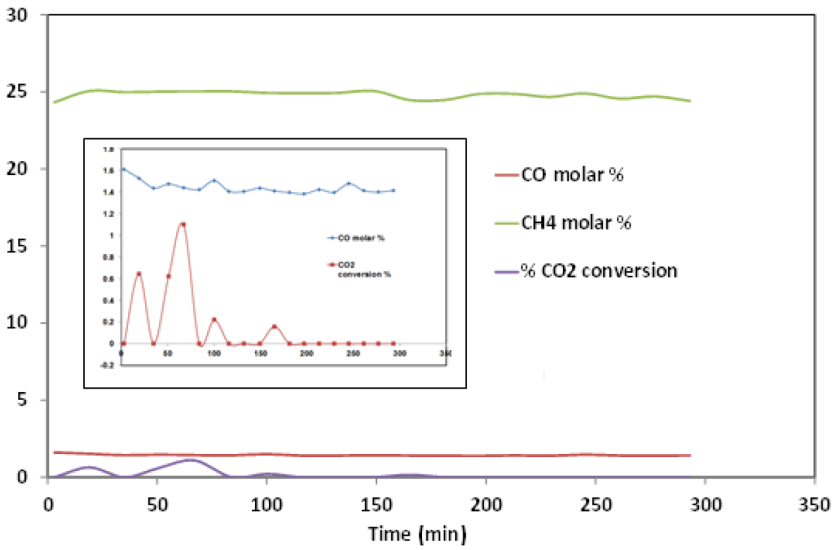

Figure 8. Deactivation results as a function of the time for the selective CO methanation over the NiCeZr-S catalysts (1% CO, 25% CO_2, 50% H_2, and rest He; S.V.: 45,000 h^{-1}; 25 mg of catalysts; T: 300 °C).

In conclusion, in this study NiO/CeO_2ZrO_2 and $Co_3O_4/CeO_2/ZrO_2$ catalysts were prepared by 3 different methods. The best surface area value was obtained from the catalysts prepared by surfactant-assisted co-precipitation with ultrasound mixing. Ultrasound mixing leads to catalysts with smaller pore diameters and higher pore volumes. Temperature programmed reduction analysis showed that surfactant leads to an

increase in the resistance to hydrogen reduction of the catalysts. Over the CoCeZr–S, CoCeZr–U, NiCeZr–S, and NiCeZr–U catalysts, all CO converted to CH_4 at ≈225 °C. Selective CO methanation was carried out over the NiCeZr–S catalyst. Above 300 °C methanation activity decreased because of the reverse water gas shift reaction. Moreover, 22.3% CH_4 formation was observed and CO level decreased under 100 ppm at 200 °C over the NiCeZr–S catalyst.

3. Experimental

The 50/25/25 (mol %) $NiO/CeO_2/ZrO_2$ and 50/25/25 (mol %) $Co_3O_4/CeO_2/ZrO_2$ catalysts were prepared by the 3 different methods described below. Characteristic properties were determined using different techniques. Finally, methanation studies were carried out to investigate the effects of the catalyst preparation methods on the activity.

3.1. Catalyst preparation

All catalysts were prepared using 3 different techniques. A detailed explanation of the methods is given below.

3.1.1. Co-precipitation

$Co(NO_3)_2.6H_2O$ (Fluka, 99.0%), $Ni(NO_3)_2.6H_2O$, and $Zr(NO_3)_2.xH_2O$ (Sigma, 99%, $CeN_3O_9.6H_2O$ (Sigma, 99%) were dissolved in distilled water to achieve the desired molar ratios. Total concentration of the metals in the final aqueous solution was 0.1 M. The metal salt solution was put into a stirrer. Na_2CO_3 (1 M) solution was added to the metal salt solution to obtain a pH of the solution of 8. The precipitates were aged for 3 h at pH 8, and then filtered and washed with hot distilled water several times in order to remove excess ions. They were air dried overnight at 110 °C. Finally, the catalysts were calcined in air at 500 °C for 3 h. The co-precipitation technique was termed "C".

3.1.2. Surfactant-assisted co-precipitation

First, 6 mmol of cetyltrimethylammoniumbromide (CTAB) was dissolved in 200 mL of deionized water for 15 min using a mechanical stirrer. Then the desired amount of metal salt solution was added to CTAB solution under vigorous stirring. After this solution was mixed for 0.5 h, sodium hydroxide solution was added to it at a flow rate of 0.2 mol/L until the pH value of the solution reached 10. After this solution was mixed for 12 h, it was aged for 3 h at 90 °C. Then the solution was filtered. The precipitate was washed with hot distilled water several times in order to remove excess ions. Then the precipitate was air dried overnight at 110 °C. Finally, the catalysts were calcined in air at 500 °C for 3 h. The surfactant-assisted co-precipitation technique was termed "S".

3.1.3. Surfactant-assisted co-precipitation with ultrasound mixing

First, 6 mmol of cetiyltrimethylammoniumbromide (CTAB) was dissolved in 200 mL of deionized water for 15 min using an ultrasound stirrer. Then the desired amount of metal salt solution was added to CTAB solution under vigorous stirring. After this solution was mixed for 0.5 h, sodium hydroxide solution was added to this solution at 0.2 mol/L flow rate until the pH of the solution was 10. After this solution was mixed for 12 h, it was aged for 3 h at 90 °C using both mechanical and ultrasound stirrers. The stirring period was adjusted as 20 min ultrasound stirrer + 40 min mechanical stirrer + 20 min ultrasound stirrer + 40 min mechanical stirrer + 20 min ultrasound stirrer + 40 min mechanical stirrer. Then the solution was filtered. Then the precipitate

was washed with hot distilled water several times in order to remove excess ions. They were air dried overnight at 110 °C. Finally, the catalysts were calcined in air at 500 °C for 3 h. The surfactant-assisted co-precipitation with ultrasound mixing technique was termed "U".

3.2. Catalyst characterization

Different techniques were used in order to determine the physical properties of the catalysts: X-ray diffraction (XRD), N_2 adsorption, temperature programmed reduction (TPR-H_2), scanning electron microscopy (SEM), and transmission electron microscopy (HRTEM). The BET multipoint surface areas, pore volumes, and pore diameters of the catalysts were evaluated by using a Quantochrome Autosorp 1C/MS device. Before the analysis, the samples were outgassed at 300 °C for 1 h. Average pore sizes were determined using the BJH method. X-ray diffraction patterns were obtained using a PHILIPS PW 1840 diffractometer. A Rigaku rotating anode X-ray diffractometer system generating Cu$K\alpha$ radiation was used to obtain XRD patterns. Temperature programmed reduction was carried out using a PerkinElmer Clarus 500 gas chromotograph equipped with a thermal conductivity detector (TCD). In the experiments 25 mg of catalysts was used. Before the reduction, catalyst samples were pretreated with He at 500 °C for 1 h. TPR measurement was performed after cooling the samples to room temperature in a helium flow. A gas mixture composed of 5% H_2 and 95% N_2 was used with a flow rate of 50 mL/min while the reactor was heated from room temperature to 800 °C at a heating rate of 10 °C/min. The morphology of the catalyst was examined using a NOVA NANOSEM 430 device. The morphology of the catalyst surface and the metal dispersion on the surface were determined by using TEM analysis. The TEM measurements were carried out on a JEOL 2100 HRTEM electron microscope.

3.3. Activity measurements

Catalytic activities of the catalysts were determined for the methanation reactions. All of the catalysts were tested for CO methanation activity. The selective CO methanation and deactivation tests were carried out over the catalyst that gave the best activity for CO methanation. Before the catalytic measurements, fresh catalysts were in situ reduced under 100% H_2 atmosphere for 1 h at 500 °C. Catalytic activity measurements for the CO methanation reaction were carried out in a fixed bed quartz tubular reactor using 25 mg of catalyst. The 1% CO, 50% H_2, and rest He feed gas composition was used. The temperature range of the reactor was from 125 °C to 375 °C. The flow rate of the feed gas was 25 mL/min. The analysis of the reactor effluent was performed by an on-line PerkinElmer CLARUS 500 gas chromatograph equipped with a thermal conductivity detector (TCD). The chromatograph column packing was carbosphere and the column temperature was maintained at 50 °C. The selective CO methanation reaction was performed by using feed gas with a composition of 1% CO, 25% CO_2, 50% H_2, and the rest He while the reactor temperature was changed from 100 °C to 600 °C. The deactivation test was carried out over the most active catalyst for CO methanation. The reaction temperature was kept constant at 300 °C for ≈300 min by using the 1% CO, 25% CO_2, 50% H_2, and rest He gas mixture.

The CO and CO_2 conversions were calculated by using the equations given below.

$$\text{For the CO methanation: \% CO Conversion} = \frac{[CO]_0 - [CO]_f}{[CO]_0} \times 100$$

$$\text{For the } CO_2 \text{ methanation: \% } CO_2 \text{ Conversion} = \frac{[CO_2]_0 - [CO_2]_f}{[CO_2]_0} \times 100,$$

where $[CO]_0$ = the inlet CO concentration in the feed gas, $[CO]_f$ = the outlet CO concentration, $[CO_2]_0$ = the inlet CO_2 concentration in the feed gas, and $[CO_2]_f$ = the outlet CO_2 concentration.

Acknowledgments

The authors gratefully acknowledge the financial support from the Gazi University BAP18/2008-01 and TÜBİTAK 109M230 projects. We are also grateful to Prof Dr Çiğdem Güldür for her help in providing equipment.

References

1. Habazaki, H.; Yamasaki, M.; Zhang, B. P.; Kawashima, A.; Konho, S.; Takai, T.; Hashimoto, K. *Appl. Catal. A-Gen.* **1998**, *172*, 131–140.
2. Fujita, S. I.; Takezawa, N. *Chem. Eng. J.* **1977**, *68*, 63–68.
3. Xavier, K. O.; Sreekala, R.; Rashid, K. K. A.; Yusuf, K. K. M.; Sen, B. *Catal. Today* **1999**, *49*, 17–21.
4. Xu, G.; Chen, X.; Zhang, Z. G. *Chem. Eng. J.* **2006**, *121*, 97–107.
5. Galletti, C.; Specchia, S.; Sorocco, G.; Specchia, V. *Int. J. Chem. React. Eng.* **2007**, *5*, Article A110.
6. Moretti, E.; Storaro, L.; Talon, A.; Lenarda, M.; Riello, P.; Frattini, R.; Yuso, M. V. M.; Jiménez-López, A.; Rodríguez-Castellón, E.; Ternero, F.; et al. *Appl. Catal. B- Environ.* **2011**, *102*, 627–637.
7. Xu, R.; Wang, X.; Wang, D.; Zhou, K.; Li, Y. *J. Catal.* **2006**, *237*, 426–430.
8. Gómez, L. E.; Tiscornia, I. S.; Boix, A. V.; Miro, E. E. *Int. J. Hydrogen Energ.* **2012**, *37*, 14812–14819.
9. Takenaka, S.; Shimizu, T.; Otsuka, K. *Int. J. Hydrogen Energ.* **2004**, *29*, 1065–1073.
10. Choudhury, M. B. I.; Ahmed, S.; Shalabi, M. A.; Inui, T. *Appl. Catal. A- Gen.* **2006**, *314*, 47–53.
11. Panagiotopoulou, P.; Kondarides, D. I.; Verykios, X. E. *Appl. Catal. A- Gen.* **2008**, *344*, 45–54.
12. Zhou, G.; Lu, M.; Gu, F.; Wang, S.; Xiu, Z. *Mater. Lett.* **2005**, *59*, 2706–2709.
13. Streethawong, T.; Yamada, Y.; Kobayashi, T.; Yoshikawa, S. *J. Mol. Catal. A- Chem.* **2005**, *241*, 23–52.
14. Liu, H.; Ma, Z.; Chu, Y.; Sun, W. *Colloids and Surfaces A: Physicochemical Engineering Aspects* **2006**, *287*, 10–15.
15. Laosiripojana, N.; Assabumrungrat, S.; Charojrochkul, S. *Appl. Catal. A- Gen.* **2007**, *327*, 180–188.
16. Laosiripojana, N.; Sutthisripok, W.; Assabumrungrat, S. *Chem. Eng. J.* **2007**, *127*, 31–38.
17. Ganesan, R.; Ham, D. J.; Lee, J. S. *Electrochem. Commun.* **2007**, *9*, 2576–2579.
18. Yang, H. M.; Chen, Y. C. *J. Taiwan Inst. Chem. E.* **2012**, *43*, 897–903.
19. Chung, H. T.; Hsiao, H. C.; Weng, H. S. *J. Chin. Inst. Chem. Eng.* **2008**, *39*, 449–455.
20. Li, H.; Zhang, J.; Li, H. *Catal. Commun.* **2007**, *8*, 2212–2216.
21. Lin, S. S. Y.; Daimon, H.; Ha, S. Y. *Appl. Catal. A- Gen.* **2009**, *366*, 252–261.
22. Khaodee, W.; Jongsomjit, B.; Assabumrungrat, S.; Praserthdam, P.; Goto, S. *Catal. Commun.* **2007**, *8*, 548–556.
23. Fischer, N.; Van Steen, E.; Claeys, M. *Catal. Today* **2011**, *171*, 174–179.
24. Takeguchi, T.; Furukawa, S.; Inoue, M. *J. Catal.* **2011**, *202*, 14–24.
25. Asencios, Y. J. O.; Assaf, E. M. *Fuel Process. Technol.* **2013**, *106*, 247–252.
26. Sing, K. S. W.; Everett, D. H.; Haul, R. A. W.; Moscou, L.; Pierotti, R. A.; Rouquerol, J.; Siemieniewska, T. *International Union of Pure and Applied Chemistry* **1985**, *57*, 603–619.
27. Pavasupree, S.; Ngamsinlapasathian, S.; Pivsa-art, S.; Suzuki, Y.; Yoshikawa, S. *Asian J. Energ. Environ.* **2005**, *6*, 193–201.
28. Tsoncheva, T.; Ivanova, L.; Micchev, C.; Froba, M. *J. Colloid Interf. Sci.* **2009**, *333*, 277–284.
29. Cao, J. L.; Wang, Y.; Zhang, T. Y.; Wu, S. H.; Yuan, Z. Y. *Appl. Catal. B- Environ.* **2008**, *78*, 120–128.
30. Jiang, H.; Meng, X.; Dai, H.; Deng, J.; Liu, Y.; Zhang, L.; Zhao, Z. *J. Hazard. Mater.* **2012**, *217–218*, 92–99.

31. Xuehong, Z.; Rui, W.; Licheng, L.; Honxing, D.; Guizhen, Z.; Hang, H. *Chin. J. Catal.* **2011**, *32*, 827–835.
32. Hernandez, M. L.; Montoya, J. A.; Del Angel, P.; Hernandez, I.; Espinosa, G.; Lianoz, M. E. *Catal. Today* **2006**, *116*, 169–178.
33. Boffito, D. C.; Crocella, V.; Pirola, C.; Neppolian, B.; Cerrato, G.; Ashokkumar, M.; Bianchi, C. L. *J. Catal.* **2013**, *297*, 17–26.
34. Lee, J., Ashokkumar, M., Kentish, S. E. *Ultrason. Sonochem.* **2014**, *21*, 60–68.
35. Guo, Z., Jones, A. G., Li, N., Germena S. *Powder Technol.* **2007**, *171*, 146–153.
36. Okkay, H., Bayramoğlu, M., Öksüzömer, M. F. *Ultrason. Sonochem.* **2013**, *20*, 978–983.
37. Cai, X.; Cai, Y.; Lin, W. *J. Nat. Gas Chem.* **2008**, *17*, 201–207.
38. Li, H.; Wang, J. *Chem. Eng. Sci.* **2004**, *59*, 4861–4867.
39. Li, H.; Xu, H.; Wang, J. *J. Nat. Gas Chem.* **2011**, *20*, 1–8.
40. Dajiang, M.; Yaoqiang, C.; Junber, Z.; Zhenling, W.; Di, M.; Maochu, G. *J. Rare Earths* **2007**, *25*, 311–315.
41. Lertwittayanon, K.; Atong, D.; Aungkavattena, P.; Wasanapiarnpong, T.; Wada, S.; Sricharoenchaikul, V. *Int. J. Hydrogen Energ.* **2010**, *35*, 12277–12285.
42. Wang, N.; Chu, W.; Zhang, T.; Zhaou, X. S. *Chem. Eng. J.* **2011**, *170*, 457–463.
43. Yongzhao, W.; Ruifang, W.; Yongxiang, Z. *Catal. Today* **2010**, *158*, 470–474.
44. Batista, M. S.; Santiago, E.; Assaf, E. M.; Ticianelli, E. A. *J. Power Sources* **2005**, *145*, 50–54.
45. Wu, R. F.; Zhang, Y.; Wang, Y. Z.; Gao, C. G.; Zhao, Y. X. *J. Fuel Chem. Technol.* **2009**, *37*, 578–582.
46. Liu, Q.; Dong, X.; Sons, Y.; Lin, W. *J. Nat. Gas Chem.* **2009**, *18*, 173–178.
47. Wang, Y.; Wu, R.; Zhao, Y. *Catal. Today* **2010**, *158*, 470–474.
48. Zhang, H.; Dong, Y.; Fang, W.; Lian, Y. *Chinese J. Catal.* **2013**, *34*, 330–335.
49. Zyryanova, M. M.; Synthikov, P. V.; Amasov, Yu. I.; Kuzmin, V. A.; Kirilov, V. A.; Sobyanin, V. A. *Chem. Eng. J.* **2011**, *176–177*, 106–113.
50. Jiang, M.; Wang, B.; Yao, Y.; Wang, H.; Li, Z.; Ma, X.; Qin, S.; Son, Q. *Appl. Catal. A- Gen.* **2014**, *469*, 89–97.
51. Liu, Q.; Dong, X.; Mo, X.; Lin, W. *J. Nat. Gas Chem.* **2008**, *17*, 268–272.